JOURNAL OF MATERIALS SCIENCE 30 (1995) 2571–2576

Effect of specimen thickness on the impact resistance of alumina

R. M. ANDERSON, G. LAIRD II, J. A. HAWK
US Bureau of Mines, Albany Research Center, 1450 Queen Avenue, SW, Albany, OR, USA

During the course of an ongoing study into the impact and erosion properties of alumina by the US Bureau of Mines, it was discovered that specimen thickness had a significant effect upon certain fractographic observations. To quantify this effect, impact studies were carried out on 1.9, 3.1 and 10.0 mm thick Al_2O_3 (alumina) discs. These discs were impacted at velocities from 15 to 65 m s^{-1} using 1.69 mm-diameter WC–Co spheres. In conjunction with this experimental approach, finite element models of the impact couples were constructed for the 1.9 and 10.0 mm-thick alumina discs. An elastic/plastic analysis was performed of the impact event in each case. Experimental and numerical results indicate that the length, depth and geometry of radial cracks are strongly dependent upon specimen thickness.

1. Introduction

Advanced structural ceramics, such as Al_2O_3 and Si_3N_4, possess both high strength and superior high-temperature properties. Such a unique combination of properties make these ceramics attractive for high-temperature structural components and as wear components for low impact, high abrasion environments. Typically ceramics are brittle, with the fracture stress controlled by the size of the flaws within the component. These flaws may be intrinsic due to processing conditions or extrinsic, i.e. caused by handling or conditions encountered during service. Impact with either blunt or sharp projectiles may also be a significant source of flaws in ceramics, leading to a shorter wear life or the premature failure of the structural component [1, 2]. The US Bureau of Mines is studying this impact process in order to understand, and thereby improve, the impact response of commercially available fine grained Al_2O_3 (alumina).

Inelastic impact and static indentation events of sufficient magnitude will normally produce radial cracks [3–5]. Inasmuch as they form on a plane perpendicular to the surface, radial cracks are considered to be strength-determining primary flaws [6–8]. That is, upon subjecting the test specimen to a tensile stress field, fracture will originate and propagate from the dominant radial or cone crack, leading to failure of the test specimen. Moreover, predictions of residual strength versus impact event can often be made once the relationship between radial crack size and impact velocity is established [9, 10]. This relationship can be complicated for high impact velocities, i.e. when dynamic conditions apply. However, for impact velocities less than approximately 100 m s^{-1}, quasi-static conditions hold [8-11]. For a given projectile-target couple, under Hertzian quasi-static conditions, the length of the radial crack is predicted to be proportional to $v^{4/5}$ [12]. Kirchner *et al.* [13] obtained qualitative agreement using this formula for radial cracks measured on 3 mm-thick zirconia plates impacted by WC–Co spheres. However, at velocities greater than 60 m s^{-1} the radial crack lengths were much longer than expected. We also noted this same anomalous radial crack length behaviour for 1.9 and 3.1 mm-thick Al_2O_3 disks impacted with WC–Co spheres but not for the 10.0 mm-thick discs. Interestingly, it appears that the impact fracture response is governed more by the specimen geometry, i.e. the disc thickness, than by the inherent toughness of the target material. This conundrum forms the basis of our investigation.

2. Experimental procedure

Commercial 99.5 alumina was obtained in the form of a 30.0 mm-thick plate. From this plate, cylinders (29 mm in diameter) were cut using a core drill. Discs 1.9, 3.1 and 10.0 mm thick were sliced from these cylinders. The ends were then polished to a 1/4 micron diamond finish using standard metallographic procedures. Impact experiments were performed using a gas gun and 1.69 mm WC–Co (6 wt % Co) spheres [14]. The impact velocities ranged from 15–65 m s^{-1}. An optical microscope was used to measure the length of the radial cracks and the diameter of the impact craters.

Strength tests were conducted using a three ball biaxial flexure fixture described by Wachtman *et al.* [15] with displacements applied via a screw-driven load frame at a crosshead speed of 8.3×10^{-5} m s^{-1}. A 25 kN load cell was used to record loads. Prior to strength testing, several impacted specimens were immersed in dye penetrant to define the subsurface radial crack geometry.

A finite element analysis was used to determine the effect of specimen thickness on the post-impact or residual stress distribution. The residual stress field

0022–2461

results from the inelastic nature of the impact or indentation event. That is, during impact, a small amount of plastic flow occurs beneath and around the impacting sphere. Finite element modelling of elastic/plastic contact is a well established procedure [16–19]. A typical axisymmetric finite element model used in this study is shown in Fig. 1. The sphere and disc were modelled using four-node isoparametric elements [20] with gap elements [21] employed between the sphere and disc to transfer contact forces. Constitutive and kinematic relationships were modelled using small strain theory with a bilinear elastic/plastic material response [20]. Elastic modulus and yield strength for the WC–6%Co sphere were 640 GPa, and 5.2 GPa, respectively [22]. Whereas for the alumina, the elastic modulus is 370 GPa [23] with a pseudo yield strength (flow stress ≈ yield stress) inferred from hardness measurements [24] as approximately 3.9 GPa. Poisson's ratio for WC–6%Co and alumina were approximated at 0.25. The work hardening response of both the WC–6%Co and alumina were assumed to be negligible [25]. However, to enforce convergence within the numerical procedure a tangent hardening modulus of 1% of the elastic modulus was used for both materials.

Finite element models were constructed to simulate impact of the 1.9 mm- (Fig. 1) and 10.0 mm-thick alumina specimens. Boundary conditions along the bottom of the plates were enforced by additional gap elements that only resist compressive forces. The modelled impact event was simulated as behaving quasi-statically and hence, all dynamic stress wave effects were ignored.

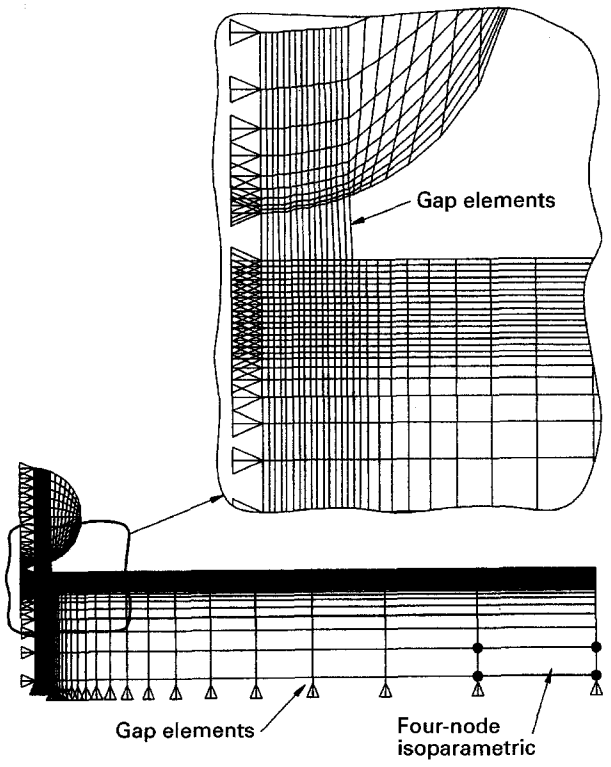

Figure 1 Axisymmetric finite element model of a 1.69 mm-diameter WC–6%Co sphere and 20 mm diameter, 1.9 mm-thick alumina disc.

3. Results and discussion

Fig. 2 is a plot of crater diameter versus impact velocity for the three thicknesses of alumina discs. For the limited range of velocities studied, the relationship between crater diameter and impact velocity is linear. Typically, the contact diameter is proportional to $v^{2/5}$ over a wide range of velocities for elastic contact (i.e. Hertzian cone fracture theory) [26]. The relationship between crater diameter and impact velocity was unaffected by the thickness of the specimen for velocities between 15 and 65 m s^{-1}. However, as evidenced in Fig. 3, the length of the radial cracks is significantly influenced by the specimen thickness. For the 10.0 mm-thick specimen the radial crack length increases in an approximately linear manner with impact velocity. This is in good agreement with the earlier mentioned theoretical predictions [12, 13]. Additionally, the radial crack lengths on the 3.1 mm-thick specimen are similar to

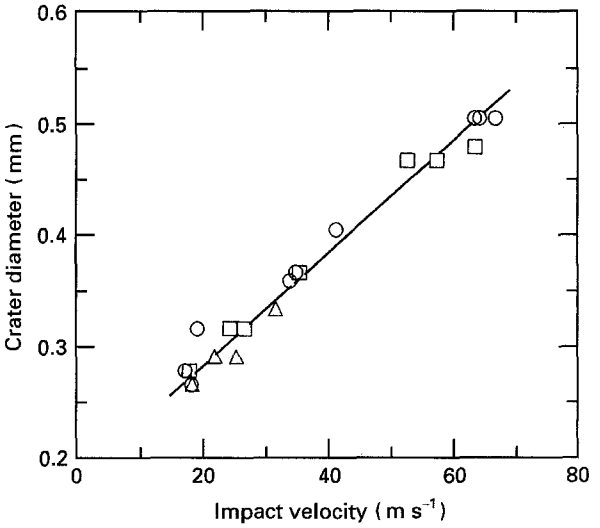

Figure 2 Crater diameter versus impact velocity (1.69 mm-diameter WC–6%Co sphere) for the three thicknesses of alumina discs. ○ 10 mm; □ 3.1 mm; △ 1.9 mm.

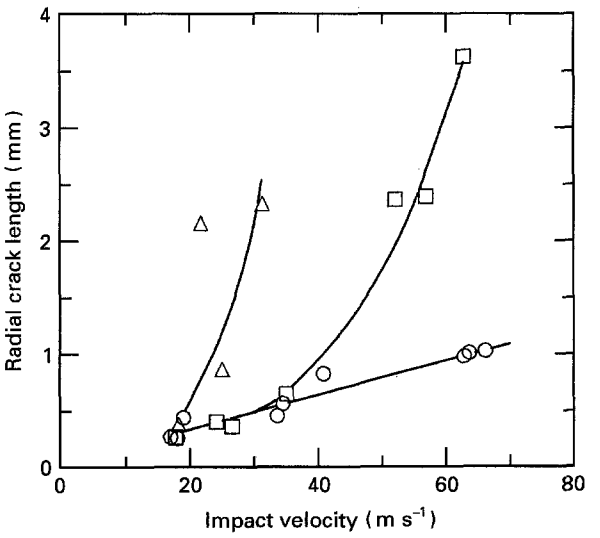

Figure 3 Radial crack length as measured using an optical microscope versus impact velocity (1.69 mm-diameter. WC–6%Co sphere) for the three thicknesses of alumina discs. ○ 10 mm; □ 3.1 mm; △ 1.9 mm.

those on the 10.0 mm-thick specimen up to impact velocities of $\sim 40\ m\ s^{-1}$. At higher impact velocities the crack lengths become much longer than those found on the 10.0 mm-thick specimen. For the thinnest alumina discs (1.9 mm thick), crack lengths were similar to the 3.1 and 10.0 mm-thick samples only at the lowest velocity ($\sim 15\ m\ s^{-1}$). Above this velocity threshold, the crack size increases rapidly with impact velocity. At the highest velocities it was usual to see 10–15 radial cracks around the impact crater.

Analysis of radial crack lengths for the three specimens reveals that: (i) for the 3.1 and 10.0 mm-thick samples the ratio of the longest crack to an average of the five longest cracks is approximately 1.2; whereas, (ii) for the 1.9 mm-thick specimens this ratio increased to a maximum of 2.2 with 1 or 2 of the radial cracks being much longer.

3.1. Crack geometry

For the 1.9 and 3.1 mm-thick alumina discs, the radial crack length can easily exceed the specimen thickness. If a typical half-penny crack morphology is assumed, then it would be expected that the specimen will immediately fall apart upon impact. However, it was observed that the impacted specimens remained intact and retained a significant amount of their strength, approximately 65% for the sample with the longest crack compared to the one with the shortest crack (Fig. 4). This result requires a change in subsurface geometry from the half-penny crack type observed for short cracks in the 10.0 mm-thick discs to an elongated elliptical geometry in the thinner discs (Fig. 5). To verify this mechanism, radial crack geometries were observed by staining the crack plane with a dye penetrant prior to strength testing (fracture). It was found that, in general, the short secondary radial cracks as well as longer radial cracks on the 10.0 mm-thick specimens, possess approximately quarter-penny geometry (i.e. they are often not coplanar with their diametrically opposed counterpart). Alternately, the radial crack length geometries for the 1.9 and 3.1 mm-thick specimens were found to be elliptical with decreasing a/c ratios as the crack length increases (a is the radial crack depth and c is the radial crack length). Importantly, fracture surfaces produced by linking short and long radial cracks reveal that both cracks have approximately the same depth. Overall, the crack depth for long cracks on the 1.9 and 3.1 mm-thick specimens are within 20% of the depth for the 10.0 mm-thick specimens, while the radial crack length increases as the thickness of the disc decreases.

3.2. Strength measurements

Biaxial flexure strength tests were performed on impacted 3.1 and 10.0 mm-thick specimens. A wide range of radial crack lengths were observed on these specimens as previously discussed. The fracture stress from the biaxial flexure test is calculated from the following equation [15]

$$S = -\frac{3}{4\pi}\frac{P}{d^2}(X - Y) \qquad (1)$$

where X and Y are functions of Poisson's ratio, the radius of the support circle, the radius of the loaded area, and the radius of the specimen. P is the applied load and d is the disc thickness. As previously mentioned, a value of 0.25 was used for Poisson's ratio while the specimen thickness varied from 1.9 to 10.0 mm. The radius of the support circle was 12.7 mm, the radius of the loaded area was 0.8 mm, and the radius of the specimen was 15.9 mm. Using the equations in Ref. 15, the values for X and Y were calculated to be -7.49 and 1.17, respectively. Since all biaxial flexure tests used the same specimen geometry, the quantity $(X - Y)$ was the same in all instances.

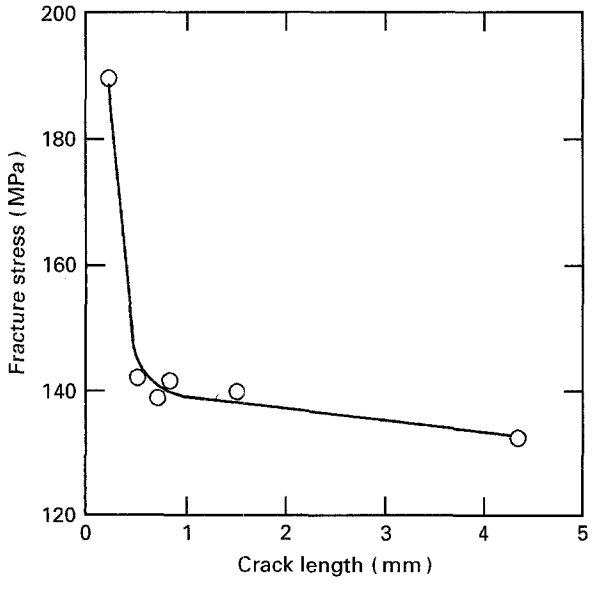

Figure 4 Fracture stress measured from biaxial strength test versus crack length for impacted 3.1 and 10.0 mm-thick alumina discs.

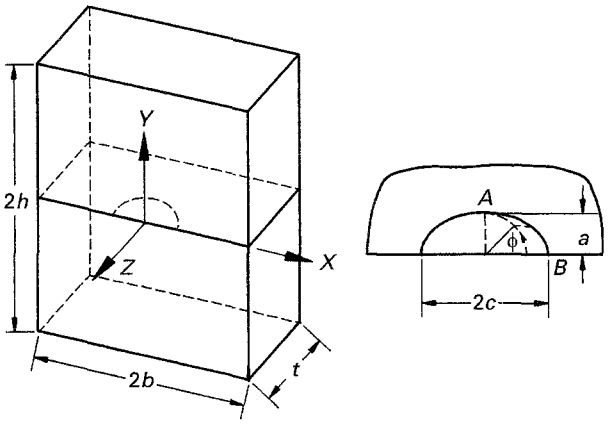

Figure 5 Schematic diagram of a finite plate with the geometry of both the half-penny and elliptical cracks shown. For the case of the half-penny crack pattern, the crack depth a or c is equal to half the surface crack length $2c$. For the elliptical crack pattern, the depth is denoted as a while the surface crack length is equal to $2c$ [27].

3.3. Stress intensity factor calculations

An estimated mode I stress intensity factor was calculated based on an equation of the form

$$K_I = Y\sigma\sqrt{c} \quad (2)$$

where Y is a crack geometry constant, σ is the applied stress and c is the characteristic crack dimension. For the half-penny crack geometry, Y is approximately 1.24 [28] and c is the radius of the half-penny crack or the length of the radial crack. In order to more accurately describe the actual crack geometry in the alumina samples, an empirical formulation developed by Newman and Raju [29, 30] is used which gives the stress intensity factors for elliptical surface cracks as a function of parametric angle, crack depth, crack length, plate thickness, and plate width for both tension and bending

$$K_I = \sigma\left[\pi\frac{a}{Q}\right]^{1/2} F\left(\frac{a}{t}, \frac{a}{c}, \frac{c}{b}, \phi\right) \quad (3)$$

In Equation 3 F and Q are empirical functions designed to correct for stress intensity at the boundary for tension and bending, respectively. The function F is obtained from a curve fitting procedure in terms of a/c, a/t, and the angular function ϕ. The terms in Equation 3 have the following meaning: a is the depth of the surface crack (for a half-penny crack a would be the radius of the crack; and for elliptical cracks, a is 1/2 the length of the minor axis), c is the half-length of the trace of the crack on the surface, t is the plate thickness, b is the half-width of the cracked plate, and ϕ is the parametric angle of the elliptical crack in the plate. Fig. 5 shows the details describing the geometry of an elliptical crack in a plate. Additional discussion on the development of this equation is found in references [27, 29, 30] and will not be discussed further. Because K_I varies along an elliptical crack front, ϕ determines the angular location for this calculation.

Using Equations 2 and 3, mode I stress intensity factors (K_I) were calculated for elliptical cracks with varying a/c ratios and for half-penny cracks with the same radial crack length or c value. Fig. 6 plots K_I for both the half-penny and elliptical ($\phi = 0.0$ (surface) and $\phi = \pi/2$ (bottom)) cracks versus radial crack length. Fig. 6 was formulated using a value of 3.1 mm for d. In addition, a crack depth of 1.55 mm (i.e. the half-thickness of the disc) was used for the elliptical cracks, regardless of the radial crack length. For the half-penny crack, the length of the radial crack corresponds to its depth. It can be seen that the stress intensity factor for a half-penny crack continues to increase as the length of the crack increases. However, for the elliptical crack geometry, the stress intensity factor for the crack converges to approximately 3 MPa $m^{1/2}$ for increasing radial crack length, whether at the surface ($\phi = 0$) or at the root of the crack ($\phi = \pi/2$). If a critical fracture toughness (K_{Ic}) of say 4.0 MPa $m^{1/2}$ is assumed for alumina, then the half-penny crack geometry would unequivocally cause fracture during impact, where the velocity exceeds 40 m s^{-1} for the 3.1 mm-thick disc (Fig. 3). Note that impact velocities for the WC–Co spheres greater than 50 m s^{-1} caused radial cracks in excess of 2 mm. These samples remained intact as did the 1.9 mm-thick alumina discs for all impact velocities used in this research. Therefore, it appears reasonable to use an elliptical crack geometry for K_I calculations. Additionally, whether the elliptical geometry K_I is calculated at the bottom of the crack or at the surface, the value of stress intensity remains less than that for the equivalent half-penny crack.

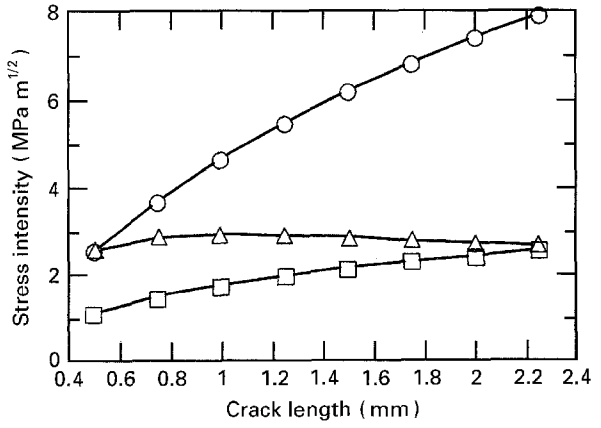

Figure 6 Mode I stress intensity factor calculations for half-penny and elliptical crack geometries as a function of radial crack length. Specimen thickness was 3.1 mm and it was assumed that a constant crack depth a of 1.55 mm held – regardless of radial crack length. ○ half-penny; □ elliptical $\phi = 0$; △ elliptical $\phi = \pi/2$.

Newman and Raju [29] have generated some curves and empirical relations relating stress intensity to the angular position along the crack, ϕ. Some general trends were observed from these curves: when a/c is small (i.e. the depth of the crack is small compared to the length of the crack, or the crack is "shallow"), and only for small values of a/t (less than 0.4), the stress intensity at the crack is greater at the bottom than at the surface. In virtually all other cases, the maximum stress intensity occurs at the surface. Thus, it is expected that in bending, for typical values of a/t (e.g. 0.5) and a/c (e.g. a/c equal to 0.4, 0.6, 0.8 and 1.0), the maximum stress intensity is located at the surface. Conversely, for a constant ratio of a/c, the stress intensity increases as the thickness of the specimen increases, except at the surface. The greatest changes in stress intensity occur at the bottom of the crack. In this research, very little change in K_I occurred at the surface for the a/c values observed. Therefore, for equivalent a/c ratios in the different thickness alumina discs, we would expect the fracture toughness to be controlled by the value of the stress intensity at the surface. The ratio of a/c is typically larger in the thinner discs (as a reaches a limiting depth while c continues to increase, Fig. 3), and for equivalent disc thicknesses, the stress intensity increases as the a/c ratio increases.

3.4. Finite element modelling results

An impact velocity of 30 m s^{-1} was used in the finite element analyses to model the impact of the 1.9 and 10.0 mm-thick alumina discs. Fig. 7(a) and (b) shows the out-of-plane hoop stress for the 10.0 mm-thick

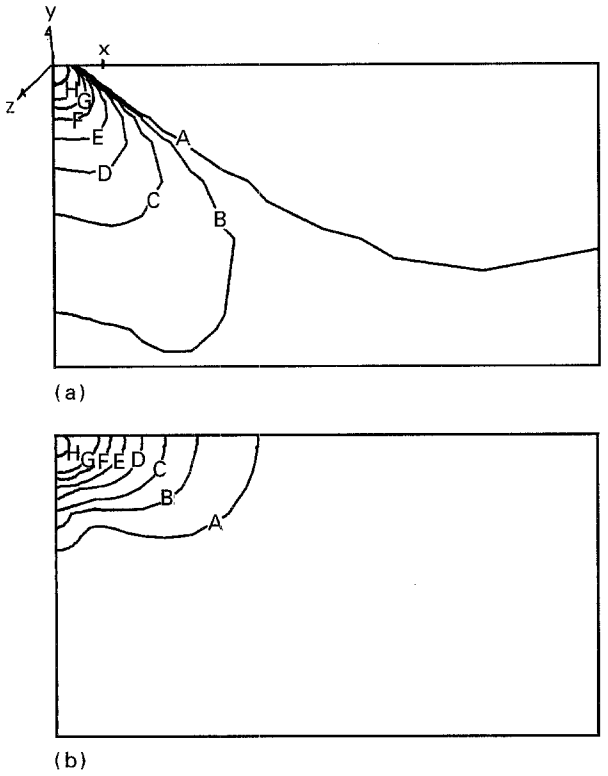

Figure 7 Finite element results showing the out-of-plane hoop stress (σ_{zz}) for the 10.0 mm-thick alumina specimen; (a) at peak impact and (b) subsequent to the impact event – no applied load. A 1 MPa; B 2.5 MPa; C 5 MPa; D 10 MPa; E 20 MPa; F 40 MPa; G 80 MPa; H 160 MPa.

alumina disc at peak impact, and subsequently, after the impact event. It is this out-of-plane hoop stress, or σ_{zz}, that drives the initiation and propagation of radial cracks. In Fig. 7(a) the stress contours are bunched around the impact area and curve downward–away from the surface. This is in direct contrast to the σ_{zz} contours shown in Fig. 7(b) which bend up to meet the surface. These results agree with the fractographic observations of Cook and Pharr [4], that radial cracks dominantly propagate during the unloading stage of the contact event.

A totally different σ_{zz} contour pattern is represented in Fig. 8(a) for the 1.9 mm-thick model at peak load when compared to that for 10.0 mm-thick model (Fig. 7(a)). However, the residual stress field patterns are somewhat similar for both the 1.9 and 10.0 mm-thick finite element models. It appears that the geometry of the specimen strongly influences the peak load stress field and to some extent the residual stress field. These results indicate (Fig. 8(a)) that the long radial cracks formed in the thin specimens (1.9 and 3.1 mm) propagate primarily during the loading phase of the impact event (Fig. 8(a)) although crack extension during unloading also occurs (Fig. 8(b)). Specifically, in the 10.0 mm-thick alumina specimen, the relative increase in radial crack length (e.g. a crack generated by $\sigma_{zz} = 10$ MPa, contour D) during unloading versus that during impact is approximately 4 to 1. Thus, a crack in the thick sample propagates primarily upon unloading. In the 1.9 mm-thick alumina sample for the same σ_{zz} (contour D), radial crack growth during the loading event is greater than

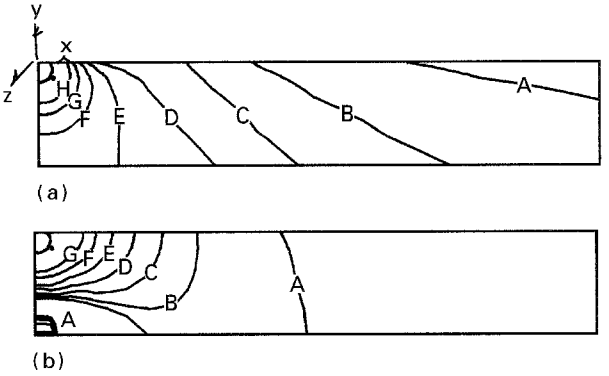

Figure 8 Finite element results showing the out-of-plane hoop stress (σ_{zz}) for the 1.9 mm-thick alumina specimen; (a) at peak impact and (b) subsequent to the impact event – no applied load. A–H as for Fig. 7.

that upon unloading. In this case, the crack only grows by 0.75 times the initial crack length. Quantitatively, the finite element results indicate that the formation of long radial cracks would be facilitated by strong σ_{zz} stress fields shown in Fig. 8(a) for thin specimens.

4. Conclusions

It was found that specimen thickness has four effects: (i) radial crack length is dependent upon the specimen thickness, e.g. as specimen thickness is reduced, radial crack length in the 1.9 mm-thick discs increases dramatically at lower impact velocities compared to the thicker discs; (ii) radial crack geometry is modified from the half-penny shape in the 10.0 mm-thick disc to an elliptical crack pattern in 3.1 and 1.9 mm-thick discs; (iii) as such, the stress intensity factor is now influenced by the specimen thickness, and long radial cracks do not necessarily mean low fracture toughness; and (iv) the results of finite element modelling quantitatively show that for thin specimens, radial crack initiation and propagation occurs primarily during the loading stage of the contact event and leads to the formation of long radial cracks.

These results have significant implications for testing the impact resistance of ceramics. Moreover, since a quasi-static approach was used, these results should hold for static indentation of strain-rate independent brittle materials. In conclusion, it seems apparent that utilizing data obtained from testing thick specimens will yield overly optimistic expectations of crack size and lead to uncertain strength predictions. Secondly, because of the potential overwhelming influence of sample thickness, the testing of relatively thin specimens is not a reliable way to assess material parameter effects on the impact resistance of ceramics.

Acknowledgements

The authors wish to thank Dr Thomas A. Adler for his careful review and Messrs Neal W. Duttlinger and Darrell P. Hoskins for their assistance with specimen preparation.

References

1. D. A. SHOCKEY, D. J. ROWCLIFFE, K. C. DAO and L. SEAMAN, *J. Amer. Ceram. Soc.* **73** (1990) 1613.
2. J. E. RITTER, *Ceramics Int.* **17** (1991) 165.
3. A. G. EVANS and T. R. WILSHAW, *Acta Metall.* **24** (1976) 939.
4. R. F. COOK and G. M. PHARR, *J. Amer. Ceram. Soc.* **73** (1990) 787.
5. R. F. COOK, B. R. LAWN and C. J. FAIRBANKS, *ibid.* **68** (1985) 604.
6. H. P. KIRCHNER and R. M. GRUVER, *Mater. Sci. Engr.* **28** (1977) 153.
7. *Idem ibid.* **28** (1977) 249.
8. A. G. EVANS, in "Treatise on materials science and technology", Vol. 16 (Academic Press, New York, 1979) p. 65.
9. H. P. KIRCHNER and R. M. GRUVER, *Mater. Sci. Engr.* **34** (1978) 25.
10. Y. AKIMUNE, Y. KATANO and K. MATOBA, *J. Amer. Ceram. Soc.* **72** (1989) 1422.
11. K. L. JOHNSON, "Contact mechanics" (Cambridge University Press, New York, 1985) p. 354.
12. D. M. RICHARD and H. P. KIRCHNER, in Proceedings of the 5th International Conference on Erosion by Solid and Liquid Impact, edited by D. Tabor (Cavendish Laboratory, University of Cambridge Press, UK, 1979) p. 27.
13. H. P. KIRCHNER, R. M. GRUVER, D. M. RICHARD and R. C. GARVIE, *Mater. Sci. Engr.*40 (1979) 49.
14. D. G. RICKERBY, B. N. PRAMILABAI and N. H. MACMILLAN, *J. Mater. Sci.* **14** (1979) 1807.
15. J. B. WACHTMAN, JR., W. CAPPS and J. MANDEL, *ibid.* **7** (1972) 188.
16. A. K. BHATTACHARYA and W. D. NIX, *Int. J. Solid Structures* **27** (1991) 1047.
17. R. HILL, F. R. S. STORÅKERS and A. B. ZDUNEK, *Proc. R. Soc. A* **423** (1989) 301.
18. T. J. LARDNER, J. E. RITTER, M. L. SHIAO and M. R. LIN, *Int. J. Fracture* **44** (1990) 133.
19. M. IMAOKA and I. YASUI, *J. Non-Crystalline Solids* **22** (1976) 315.
20. R. D. COOK, "Concepts and applications of finite element analysis, 2nd edn (Wiley, New York, 1981).
21. ANSYS Theoretical Manual, edited by P. C. Kohnke (Swanson Analysis System, Houston, PA 1989) pp. 2–12.
22. N. INGELSTROM and H. NORDBERG, *Eng. Fracture Mech.* **6** (1974) 597.
23. AD995 Coors Handout.
24. I. J. McCOLM, "Ceramic hardness" (Plenum Press, New York, 1990) p. 12.
25. A. KELLY and N. H. MACMILLAN, "Strong solids", 3rd edn (Clarendon Press, Oxford, UK, 1986) p. 140.
26. H. R. HERTZ,"Hertz's miscellaneous papers" (Macmillan, London, UK, 1896) Chs 5 and 6.
27. T. L. ANDERSON, "Fracture mechanics" (CRC Press, Boca Raton, FL, 1991) pp. 735–736.
28. R. F. COOK, C. J. FAIRBANKS, B. R. LAWN and Y. W. MAI, *J. Mater Res.* **2** (1987) 345.
29. J. C. NEWMAN, JR and I. S. RAJU, *Eng. Fracture Mech.* **15** (1981) 185.
30. I. S. RAJU and J. C. NEWMAN, JR, *J. Pressure Vessel Tech.* **104** (1972) 293.

Received 29 April
and accepted 13 October 1994